

Process intensification through Staggered Herringbone Micro-channels: mass transfer enhancement to a reactive wall

Alberto Cantu-Perez^a, Enrique López-Guajardo^{b,*}, Michel Romero-Flores^b, Krishna D.P. Nigam^{b,c}, Asterios Gavriilidis^d and Alejandro Montesinos-Castellanos^{b,*}

^aNutec-Bickley Research, Development and Innovation, Carr. Saltillo-Monterrey No. 100, Sta. Catarina, NL 66359, México; ^bEscuela de Ingeniería y Ciencias, Tecnológico de Monterrey, Campus Monterrey. Ave. Eugenio Garza Sada 2501 Sur, Monterrey Nuevo León 64849, México; ^cDepartment of Chemical Engineering, Indian Institute of Technology. Hauz Khas, New Delhi, Delhi 110016, India; ^dUniversity College London, Department of Chemical Engineering, Torrington Place, London WC1E 7JE, UK

Authors' Information

Alberto Cantu-Perez e-mail address:
albertocantu@nutec.com

Enrique A. López-Guajardo e-mail address:
enrique.alopezg@tec.mx
ORCID: 0000-0002-5728-9816

Michel Romero-Flores e-mail address:
A00818452@itesm.mx
ORCID: 0000-0001-6513-9335

Krishna D.P. Nigam e-mail address:
nigam@tec.mx; nigamkdp@gmail.com

Asterios Gavriilidis e-mail address:
a.gavriilidis@ucl.ac.uk

Alejandro Montesinos-Castellanos e-mail address:
alejandro_montesinos@tec.mx
ORCID: 0000-0001-9249-8878

Declaration of interest: Authors declare no conflict of interest

Corresponding Authors

*Enrique A. López-Guajardo e-mail address: enrique.alopezg@tec.mx
Phone Number: (+52)83582000 ext. 5561

* Alejandro Montesinos-Castellanos e-mail address: alejandro_montesinos@tec.mx
Phone Number: (+52)83582000 ext. 5280

Abstract

In the present study, the flow behaviour through different micro-herringbone channels configurations (1-peak, 2-peak, 1-2 alternated peak herringbone channel and a flow inversion geometry) have been numerically analysed as a mean of intensifying mass transfer to a reactive boundary. Results showed that the mass transfer coefficients were higher for the 1-2 alternated herringbone structure than those with, either, 1-peak or 2-peak structures. Moreover, the flow inversion structure mass transfer coefficients were double those obtained for the staggered herringbone channel. The alternated herringbone channel combines a different set of herringbone structures that are efficient at removing the boundary layer at different parts of the channel. The combination of these structures provide an enhanced mass transfer performance as compared to a standard herringbone channel. The obtained results showed that a 2D simplified model which uses hydrodynamic data from CFD simulations is a reasonable substitute for full 3D particle tracking simulations in terms of the mass transfer behavior of the 1PSHC with a 97.5% of accuracy related to the asymptotic Sherwood number. The mixing capacity of the herringbones was accounted for by an apparent effective diffusion coefficient. The agreement between the 3D and 2D simulation was reasonable.

Keywords: Mass transfer; Static mixer; Micro-channel; Reactive wall; Staggered herringbone channel.

1. Introduction

The design and implementation of disruptive technologies that leads to the reduction of: 1) the capital investment of a chemical processing plant, 2) risk of operation, 3) environmental impact and 4) energy and material consumption are part of the actions that chemical industry is taking towards a highly efficient and sustainable production scheme [1–3]. The development, design and implementation of devices that drastically improves how chemicals are produced fall within the main objectives of Process Intensification (PI). One of the strategies involved in the philosophy behind PI is the change from batch mode operation processes to continuous processes which involves modular equipment that satisfy this production scheme while reducing the equipment dimensions (millimetric or micrometric devices) and thus, increasing the selectivity of the process and quality of the products [4–6]. This miniaturization of chemical processes and equipment is becoming a growing trend in the chemical engineering field and its key towards a sustainable and green processes [7].

Due to the small dimensions of micro-size unit operation equipment, the surface to volume ratio is several orders of magnitude higher compared to conventional equipment. For this reason, the rates of heat and mass transfer are high, leading to greater space-time yields during reactions. However, for applications where the Peclet number ($Pe = \frac{vd}{D}$) is larger than 10^2 , transverse mass transfer occurs only by diffusion. Thus, ways of mixing the fluid to intensify mass transfer are needed to approach plug flow behavior.

The staggered herringbone channel (SHC) proposed by Stroock (2002) [8] has been shown to be effective for mixing intensification[9–19]. It has been found that residence time distributions (RTD) for the staggered herringbone channel are narrower

compared to a standard rectangular channel[20,21]. RTD have also been studied numerically and experimentally for micro and milli-devices [10,15,22–25].

The SHC has also been shown to be effective at increasing mass transfer to boundaries. Kirtland et al. (2006)[26] modelled and simulated mass transfer phenomena to the top wall of a channel with floor staggered herringbone structures by tracking passive tracers over a range of Peclet numbers with an instantaneous reaction occurring at the top wall. They found that the SHC had a higher mass transfer rate (~5-fold) compared to a conventional rectangular channel. It was also found that other geometries (symmetric herringbone and diagonal grooves) which do not produce a chaotic flow had mass transfer rates comparable to the herringbone channel. The symmetric herringbone and the diagonal grooves generated sufficient transverse flow (secondary flow in the cross-section perpendicular to the flow direction) to remove the boundary layer growing in the channel ceiling. Although, these structures lead to a significantly larger drop in the average concentration as compared to an unstructured rectangular channel, the staggered herringbone channel was more efficient at removing depleted reactant from the top of the channel. This could be a consequence of the formation of a single vortex in transverse direction that does not vary along the flow direction (non-chaotic flow), since the geometry does not present any extra geometrical perturbation and presents symmetry. Consequently, mixing in the bulk fluid (fluid relatively far from the reactive wall) is not a necessary indicator of the achievement of high mass transfer rates in a reactive boundary.

Yoon et al.(2006) [27] described three methods to overcome mass transfer limitation to reactive surfaces:

- (1) Removing the depleted zone through multiple periodic outlets.
- (2) Adding fresh reactants through multiple periodic inlets.

(3) Inducing transverse convective motion with herringbone structures.

It was found that approaches (1) and (2) are better at improving the reactant conversion rate. However, the pace required for operation and the pressure drop is higher than approach (3) [27]. Golden et al. (2007) [28] used grooves for redirecting the flow and enhancing the delivery of molecules from the bulk to the reacting surface, while Lopez and Graham (2008) [29] showed that shear-induced diffusion, due to different suspensions characteristics, can also enhance the mass transfer to boundaries. Therefore, Lopez and Graham (2008) [29] concluded that the most effective way to enhance mass transfer to a boundary was through a combination of herringbone structures and shear-induced diffusion. The herringbone structures were found to be effective at circulating fluid between the adsorbing wall and the bulk, whereas the shear-induced diffusion enhanced transport across the boundary layer. Static mixers are commonly used to increase heat and mass transfer and avoid temperature and concentration gradients that are detrimental for reaction applications[30–35]. However, mixers may not be the best way of enhancing heat and mass transfer to a wall, because most of these devices rely on flow splitting/recombination or flow restructuring by symmetrical components. Thus, the fully developed flow does not present any disruptions along the mixer length, resulting in a gradual increase in the boundary layer (hindering the mass transfer to the walls).

For these applications flow inverter structures (FIS) can give a better performance because they maximize the driving force by bringing material from the wall to the bulk and vice versa[36,37]. Flow inversion for process intensification was explored by Saxena and Nigam (1984)[38] and later by others for a vast range of application[37,39–46].

FIS have been used in macroscopic equipment for increasing heat transfer performance and to obtain narrow RTDs[39,47–49]. However, a comparative study of its effectiveness against different geometrical modifications of Herringbone micro-mixers is required as a mean to determine which one obtains the highest mass transfer rates to a reactive boundary. Moreover, a simple mathematical model is needed to easily predict and compare the efficiency of these complex geometric devices.

This work deals with the modelling of mass transfer process to a reactive boundary (top wall) considering an instantaneous reaction by coupling computational fluid dynamics (CFD) and particle tracking methods for different herringbone geometries: (a) 1-peak staggered herringbone channel (1PSHC); (b) conventional straight-channel (CSC); (c) flow inversion structures (FIS); (d) 2-peak herringbone channel (2PSHC); and (e) alternated 1-peak and 2-peak herringbone channel (1-2PSHC). In addition, a simplified two-dimensional model is proposed to simulate mass transfer to boundaries that uses the eddy diffusivity concept.

2. Materials and Methods

2.1 Description of Microchannel Configurations

The herringbone structures are presented in Figure 1A and are similar to the ones proposed by Stroock(2002) [8]. The channel is divided in cycles, each consisting of twelve asymmetric grooves (1 cycle is approximately $z/h = 17$). The position of the asymmetry changes every half cycle. The channel width is $W = 200 \mu\text{m}$ and the channel height is $h = 85 \mu\text{m}$. The grooves are placed at an angle $\theta = 45^\circ$ with respect to the channel width. The groove depth (added to the channel height), $g_d = 31 \mu\text{m}$, the groove width, $g_w = 50 \mu\text{m}$ and the ridge width, $r_w = 50 \mu\text{m}$ (measured along the axial direction). An alternative herringbone structure is shown in Figure 1B. Instead of having one

herringbone spanning the entire width of the channel, there are two herringbones, covering one half of the width each. Herringbones asymmetries are located at $1/3^{\text{rd}}$ and $2/3^{\text{rd}}$ of the channel width for the first half cycle and $1/6^{\text{th}}$ and $5/6^{\text{th}}$ for the second half cycle. Channel and groove dimensions are the same as in the staggered herringbone channel. Geometry in Figure 1B is a 2-peak herringbone channel (2PSHC). Finally, geometry in Figure 1A is combined with geometry in Figure 1B to form an alternated (1-peak and 2-peak) herringbone channel (1-2PSHC) as shown in Figure 1C. On odd cycles, geometry of Figure 1A is used and on even cycles geometry of Figure 1B is used. Channels with just structures like Figure 1A are also considered and this corresponds to the "standard" 1- peak staggered herringbone channel (1PSHC) by Stroock(2002) [8]. It is worth emphasizing that the width, height, groove depth and groove width remained constant for all the geometries tested. Hydraulic diameter for all the geometries remained constant for the purpose of performance comparison.

[Suggested position of Figure 1]

The flow inversion structure (FIS) shown in Figure 1D with a $W = 200 \mu\text{m}$ and $h = 85 \mu\text{m}$, has a structure in every cycle that splits the flow so that the fluid originally close to the top wall is transported to the bottom and vice versa. This transformation allows for the disruption of the velocity profiles (from fully-developed flow to developing flow) and thus, the renewal of the boundary layer at the reactive top wall. In addition a rectangular channel with $W = 200 \mu\text{m}$, $h = 85 \mu\text{m}$ is also considered (not shown). For all structures, the cycle length is $L = 1.5\text{mm}$ and the geometry is repeated periodically.

2.2 Numerical Procedure for Mass Transfer Calculations

The species concentration for a reaction occurring at the microchannel top wall can be found by solving the convection-diffusion-reaction equation coupled with the Navier-Stokes equation. However, for liquid mixing with $Pe > 10^3$, numerical errors (often called numerical diffusion) attributed to the discretization of the convective term in the convection-diffusion equation, are likely to affect the results [40]. To avoid this problem, the computation of the trajectories of massless particles convected by the flow has been used.

The cross-sectional concentration gradient induced by an instantaneous reaction on the top wall was calculated by solving the velocity field for the particular geometry and tracking the positions of massless particles. Similar approach was used by other authors[10,50,51]. It was found that 10^5 particles were enough to ensure convergence of the calculated cross-sectional concentrations. The particles are distributed proportionally to the axial velocity at the channel inlet. This condition approximates the flux of solute through the inlet plane. A random diffusive step was implemented that approximates the effect of diffusion as the time step goes to zero. The locations of the particles are computed by integrating the following stochastic differential equation[52]:

$$d\vec{x} = \vec{U}dt + \sqrt{2Ddt}\vec{\xi} \quad (1)$$

Where \vec{x} is the vector with the positions of the particles, \vec{U} is the velocity vector, t is time, D is the diffusion coefficient and $\vec{\xi}$ is a vector with random numbers with zero mean and unit variance. The Navier-Stokes and the continuity equation for the conservation of mass, are solved simultaneously with COMSOL Multiphysics 4.3 for a full cycle. The velocity field was solved using the Laminar Flow model for incompressible flow. A no-slip boundary condition was applied to all walls. A periodic boundary condition was used in order to simulate the effect of having successive cycles

by using the results of one cycle (neglecting entrance effects); the velocity profile was obtained by specifying the pressure drop of the used geometry, that is, the pressure at the outlet of the cycle is equal to the inlet pressure minus the pressure drop. The volumetric flow rate was then computed from the integration of the velocity profile at the outlet of the system. Additionally, the volumetric flow rate was evaluated as a function of the number of mesh elements. The numerical grid consisted of 44,461 tetrahedral elements and 127,248 prismatic elements calibrated for fluid dynamics with an average element quality of 0.7. Under this grid, the solution could be considered mesh independent with an average error below 0.5% with respect the outlet volumetric flow rate. The simulations were carried out in Windows 10 with Intel Xeon 2.6 GHz CPU with two processors and 80 GB-DDR3 of RAM custom computer. A total of 40 cycles were taken into account for the performance analysis. A second order-upwind scheme was used in combination with a PARDISO solver with a nested dissection multithreaded and a relative tolerance ≤ 0.001 as a convergence criterion.

The solution is exported to MATLAB where a particle tracking algorithm obtains the velocity at the position of the particle by interpolation and gets its new position by solving Eq. 1 for a fixed time step (dt). This code is set so that the velocity field obtained for the first cycle could be used over many cycles. A standard, fourth-order Runge-Kutta method with fixed time step was used to get the solution of Eq. 1. A time step corresponding to an average distance travelled $\Delta\vec{x} = 0.17h$ was found to be sufficient, as smaller time steps did not change the results significantly. The positions of the particles and their time of arrival at a particular location are recorded and the procedure is repeated over a specified number of steps. If a particle leaves the computational domain through any of the channel walls, it is reflected specularly back to the channel flow.

The instantaneous reaction at the top wall is simulated by considering that when a particle touches the channel wall it reacts with a probability of 1. The $x y z$ position of the first crossing of the reactive wall for every particle is recorded (which indicates the position where the particle reacted). Subsequent crossings are not considered in the concentration calculations. The information of whether a particle has reacted or not is kept so that cross-sectional concentrations are obtained at different lengths. The Sherwood number is calculated from the reacting flux across the boundary.[26]

$$Sh(z) = -\frac{Peh}{C_{cup}(z)} \frac{dC_{cup}}{dz} = -\frac{d \ln C_{cup}}{d \frac{z}{Peh}} = \frac{k(z)h}{D} \quad (2)$$

In other words, the Sherwood number is the relative rate of change of C_{cup} (mixing cup concentration) with respect to the non-dimensional number $\frac{z}{Peh}$. C_{cup} can be viewed as the flow-averaged bulk concentration determined as follows:

$$C_{cup} = \frac{\int C \cdot v dA}{\int v dA} \quad (3)$$

Where the term $\int C \cdot v$ represents the surface integral of the product between concentration profile and velocity profile (in the cross-sectional area of the SHC), while $\int v$ is the surface integral of the velocity profile. Concentrations are calculated by binning the particles in evenly spaced x - y bins (2 μm squares) and dividing the number of particles that have not reacted over the total number of particles in each bin.

2.3 Simplification of mass transfer calculations using turbulent theory concepts

Even though the chaotic flow induced by herringbone structures is in principle different from the complex time-dependent motion encountered in turbulent flow, we use the eddy diffusivity concept developed for turbulence to formulate an analogous effective diffusion coefficient which can be used to account for the enhanced transverse mass transfer. This approach has been used before to approximate the mass transfer

effects of herringbone channels[11]. When Fick's law is applicable and the dispersion time is large, the eddy diffusivity can be expressed:

$$E_D = \sqrt{\overline{v_y^2}} \int_0^Y R_y dy \quad (4)$$

Where $\overline{v_y^2}$ represents the average velocity between two points and R_y is the velocity correlation between two points defined as:

$$R_y = \frac{\overline{v_y v_{y+\Delta y}}}{\overline{v_y^2}} \quad (5)$$

Since molecular diffusion takes place inside and between eddies, the transport of mass should include the effect of both molecular and eddy diffusion. Since E_D is assumed to be independent of D , the combined action of molecular and turbulent transport is considered to be additive and the effective diffusion coefficient can be calculated as[53]:

$$D_{eff} = E_D + D \quad (6)$$

The result in Eq. 4 is an average velocity multiplied by a characteristic dimension. We assume that this approach of describing transport of eddies in turbulent flow can be extended to describe the convective flow induced by the herringbone structures. A similar method of calculating an enhanced dispersion has been used by MacInnes et al.(2007) [54] for a rotating device. They found that the enhanced dispersion coefficient created by the Coriolis effect could be 100 times bigger than molecular diffusion. Similar values are obtained here considering a typical diffusion coefficient of $10^{-9} \text{ m}^2/\text{s}$ (For ionic aqueous solutions). Eq. 4 gives a constant E_D for the whole channel. Since we are interested in calculating mass transfer to a boundary, it is important to get an accurate value close to it. Several publications have acknowledged the importance of getting an accurate value close to a boundary[55–57].

In this work, to obtain E_D for the 1PSHC, the transport equations are first solved in COMSOL Multiphysics as described in the previous section. The solution is exported to MATLAB where a code gets a value of the velocity in the vertical direction (u_y) averaged over the width. Rather than calculating an arithmetic average of the vertical velocity over the width, a weighted average according to the axial velocity is calculated (analogous to the mixing cup concentration):

$$\overline{u_y}|_z = \frac{\int_0^W u_y(x, y)u_z(x, y)dx}{\int_0^W u_z(x, y)dx} \quad (7)$$

E_D was calculated as a function of channel vertical height, by changing the lower limit of the integral in Eq. 4 from 0 to y so that close to the reactive wall (where y is close to h) we do not overestimate E_D . This is done in order to capture the fact that the area of interest is between the specific vertical location and the reactive wall. In addition, the constant velocity $\sqrt{\overline{u}^2}$ is replaced with u_y to account for the small velocities near the reactive wall. Eq. 7 gives the weighted vertical velocity value at a given (y, z) coordinate. A simple arithmetic average over 120 values obtained at different z locations is calculated to obtain a single value of u_y that is valid for the whole channel cycle. With this procedure a function of $E_D(y)$ is obtained.

The possibility of using this procedure to replace the effect of the herringbone structures with a D_{eff} and reduce the model from a 3-dimensional geometry to a simpler 2D model is discussed in section 3.2. This can greatly reduce the computation time and enable the simulation of more complicated geometries and reaction schemes. The mass transfer in the staggered herringbone channel can then be simulated in 2 dimensions (length and height) where the effective diffusion coefficient in the channel is calculated with Eq. 5. An 8th order polynomial is fitted to the graph of E_D vs y . This equation is used as input to a 2D model in Comsol to allow D_{eff} to change as a function of vertical

position. The Sherwood numbers are obtained from Eq. 2 using mixing cup concentrations obtained from the 2D model at different lengths. The mass transfer coefficient is then calculated from the definition of the Sherwood number.

3. Results and Discussion

Mixing enhancement and thus, hydrodynamic control is a key factor to identify possible geometrical configurations of intensified reactors. This enhancement was evaluated in terms of the capability of the geometries used to react at a fixed catalytic wall following the protocol described above. Results are discussed as follows:

3.1 Study of Mass Transfer to Boundaries with a CFD/Particle Tracking Model

The ability of the geometries shown in section 1 to improve mass transfer to the top wall is analyzed in this section. In section 3.1.1 a qualitative analysis of the effect of channel geometry on cross-sectional concentration is presented showing the cross-sectional concentrations for different channel lengths. In section 3.1.2 a quantitative comparison of the geometries is shown calculating the mixing cup concentrations and the mass transfer coefficients as a function of channel length.

3.1.1 Effect of Channel Geometry on Concentration Profiles and Reactant Conversion

Figure 2 shows the comparison of the cross-sectional reactant concentration profile for the rectangular channel, all herringbone channels (1PSHC, 2PSHC and 1-2PSHC) and FIS at different dimensionless lengths. Reactant conversion at the corresponding location is also shown. The results for the 1PSHC (~25% of conversion for $z/h=680$) are in good agreement with the literature[26]. For the 1PSHC the boundary layer forming at the top wall is partially removed by the secondary flow induced by the grooves. However, it can be seen that the material boundary layer extends primarily towards the center of the

channel. This is consistent with mixing studies of Cantu-Perez et al.(2010) [25], where it was found that the relative amount of stretching at the center of the channel was much smaller than at the sides of the channel. The zones with high stretching represent areas of good mixing. This indicates that the fluids are poorly mixed in the center of the channel which leads to the growing of the boundary layer in that region. The 1-2PSHC shows a more uniform concentration than the 1PSHC.

The presence of alternated 1-peak and 2-peak structures allows for the fluid in the center to be moved to other parts of the channel, therefore the boundary layer present in the 1PSHC is not present in the 1-2PSHC.

[Suggested position of Figure 2]

The results for the FIS show that this geometry is more efficient at removing the boundary layer than the 1PSHC. At a length of $z/h = 680$, the cross-sectional concentration profile for the FIS is nearly uniform, whereas the 1-2PSHC shows a boundary layer in the middle of the channel. However, the 1-2PSHC obtains the highest conversion of the three geometries. It is interesting to note that the improved behavior of the 1-2PSHC geometry is due to the synergy of the geometries involved (see Figure 1 A and B). It can be seen from the cross-sectional concentration profile of geometry 2PSHC, that the boundary layer grows close to the sides of the channel as opposed to the center of the channel as in the 1PSHC. On its own, the 2PSHC has worse performance than the 1PSHC (approximately half the conversion achieved in 1PSHC). However, when the structures are alternated the reaction performance is improved since the structures are complementary: the 1PSHC is good at removing material from the sides of the channel, and the 2PSHC at removing it from the center. The cross-sectional reactant concentration maps for the 1-2PSHC (see Figure 2), show regions with unreacted fluid near the center of the channel (seen as white background). The reason

for this is because all the cross-sectional maps were obtained at the end of a “2-peak structure”, and the accumulated reacted material in the center was already removed.

3.1.2 Calculation of Mass Transfer Coefficients

Figure 3A shows the mixing cup concentration calculated at different lengths for all geometries. The concentration decay for the FIS is much steeper than for the 1PSHC, with the 1-2PSHC having the steepest gradient. This is further supported by the calculated Sherwood number (Sh) shown in Figure 3B. For the 1PSHC, the Sh achieves an asymptotic value (Sh_{∞}) of 9.3 at $z/h \approx 41$. On the other hand, the FIS has $Sh \sim 15.3$ nearly twice that calculated for the 1PSHC. It is not clear whether the 1-2PSHC has reached an asymptotic value. However, for all the lengths studied the Sherwood number was about three times higher ($Sh \sim 35$) than the 1PSHC and twice as much as the one calculated for the FIS. In Figure 3A, the mixing cup concentration drops exponentially after the first 2 cycles ($z/h = 34$) which may indicate that the mass transfer coefficient is reaching a constant value, therefore, reaching an asymptotic value of Sherwood number (as seen in Figure 3B).

The 1-2PSHC shows a sudden change in the behavior of the Sherwood number with channel length. Before the end of the first cycle, the behavior is similar to the 1PSHC. However, after the first cycle a sudden increase in the Sherwood number is seen. The reason for this is because at this channel length, instead of repeating 1-peak geometry for the second cycle, 2-peak geometry is used and the mass transfer performance is improved. That is, at the 1-P section of the SHC, two asymmetric vortices (one larger than the other) are formed in the cross-sectional area. These vortices change sides at the end of half cycle by changing the asymmetry of the 1-peak. Therefore, having a 2-peak configuration leads to a disruption of the formed vortices, increasing the chaotic advection until the flow is fully developed at the end of the cycle.

It is important to note that, although the Sherwood number for the FIS is higher than the 1PSHC, the pressure drop is 2.5 times larger whereas the 1-2PSHC has a pressure drop similar to that of the 1PSHC case. This result indicates that the 1-2PSHC not only gives the highest performance in terms of mass transfer, but also has a low-pressure drop (even lower than the CSC of the same dimensions).

[Suggested position of Figure 3]

Therefore, the 1-2 PSHC and FIS are suitable for carrying out mass-transfer limited reactions, specifically reaction that take place in a catalytic wall. Nonetheless, these type of microchannels could be used for systems that requires a control on temperature and/or a low concentration gradient to successfully carry out a reaction; This control is possible due to the formation of the transverse flow and the change in direction generated from these geometries.

3.2 Study of Mass Transfer to Boundaries with Simplified 2D Model

In this section the eddy diffusivity discussed in section 2.3 is used to simplify the procedure to calculate the mixing cup concentrations and the mass transfer coefficients. Figure 4 shows the vertical velocity (u_y) calculated from Eq. 7 and virtual eddy diffusivity (E_D) as a function of channel vertical coordinate (y), averaged over the cycle length for 1PSHC. It can be seen that the strongest mixing and therefore highest E_D is close to the channel floor at around 15 to 20 μm from the floor. This is consistent with previous stretching calculations[58], where it was found that the highest stretching (highest mixing intensity) was localized close to the microchannel floor.

[Suggested position of Figure 4]

In Figure 5 the Sherwood number as a function of channel dimensionless length for the 1PSHC at different values of Pe is plotted. It can be seen that the 2D and 3D simulations agree reasonably well for $Pe = 10^4$. Furthermore, both the 3D particle

tracking and the simplified 2D model agree well with previously reported data[26]. For example, for $Pe=10^4$, the Sh_∞ reported by Kirtland et al. (2006) [26] is 8.5 (3D) while from our 3D particle tracking model is 8 and the 2D model is 7.8. The Sh_∞ in both the 3D model and the 2D model also scales with Pe as in Kirtland et al.(2006) [26]. In addition, these authors found that the evolution of the Sh scales as $Sh \propto Pe^{1/3}$, particularly on the developing region. The results obtained are consistent with the Sh scaling. Discrepancies between the 2D and 3D models are apparent at small z/h (first cycle at the same Pe). This lack of accuracy could be attributed to the nature of mass transfer variation at a given cycle, that is, the 2D model does not fully predicts the enhanced mixing taking place within the first full cycle due to the developing and disruption of the boundary layers (initial exponential decay of mass transfer coefficient). The accuracy between models increases as mass transfer reaches its asymptotic value. Nonetheless, accuracy could be improved by decreasing the time steps required and increasing the number of points at the first cycle ($z/h < 18$). Overall Figure 5 demonstrates that the 2D simplified model could predict the asymptotic Sherwood number (Sh_∞) with an accuracy of 97.5% compared to a full 3D particle tracking simulation in terms of the mass transfer behavior of the 1PSHC.

[Suggested position of Figure 5]

4. Conclusions

Mass transfer to a reactive boundary was investigated numerically for five different geometries: a 1-peak staggered herringbone channel (1PSHC), a 2-peak staggered herringbone channel (2PSHC), an alternated 1-peak and 2-peak herringbone channel (1-2PSHC), a flow inversion structure (FIS) and a conventional rectangular channel (CSC) for comparison purposes. The results indicate that the proposed 1-2PSHC is more efficient at removing the depleted reactant fluid from the reaction zone than the other

geometries, in agreement with the result the capacity for remove the depleted reactant fluid follow the relation $1-2PSHC > FIS > 1PSHC > 2PSHC > CRC$. Mass transfer coefficients were calculated for all geometries and showed good agreement with literature values. The mass transfer coefficients for the 1-2PSHC were higher at all lengths than the ones calculated for the FIS and the 1PSHC. The first set of herringbone structures in the 1-2PSHC were efficient at removing depleted reactant from the sides of the channel, while the second set of herringbones were effective at removing material from the center of the channel. The combination of the two sets resulted in higher mass transfer coefficients than the 1PSHC. The eddy diffusivity concept was used to simplify the numerical calculations. It was found that the 1PSHC could be modelled with a two-dimensional model with a virtual eddy diffusion coefficient that accounts for the stirring behavior of the herringbones. The agreement between the Sherwood numbers calculated with 3D particle tracking simulations and the 2D model was satisfactory.

Acknowledgements

The authors gratefully acknowledge Tecnológico de Monterrey, through the Energy and Climate Change Research Group and CONACYT, for the financial support of this study.

Declaration of interest statement

Authors declare no conflict of interest

Funding Source

This research is a product of the Project 266632 “Laboratorio Binacional para la Gestión Inteligente de la Sustentabilidad Energética y la Formación Tecnológica” [“Bi-National Laboratory on Smart Sustainable Energy Management and Technology

Training”], funded by the CONACYT SENER Fund for Energy Sustainability (Agreement: S0019-2014-01).

Acronyms

CSC Conventional Rectangular Channel

FIS Flow Inverter Structures

RTD Residence Time Distribution

SHC Staggered Herringbone Channel

Dimensionless numbers

Pe Peclet number = $\frac{vd}{D}$

Sh Sherwood number = $\frac{k(z)h}{D}$

Sh_{∞} Asymptotic Sherwood number

Nomenclature

C_{cup} Mixing cup concentration, mol/m³

d Characteristic dimension, m

D Diffusion coefficient, m²/s

D_{eff} Effective diffusion coefficient, m²/s

E_D Pseudo-eddy diffusivity, m²/s

g_d Groove depth, μm

g_w Groove width, μm

$k(z)$ Mass transfer coefficient, m/s

L Channel length, μm

h Channel height, μm

R_y Correlation of the velocity of particles

r_w Ridge width, μm

t Measured time, s

\vec{U} Velocity vector, m/s

$\overline{u_y}|_z$ Weighted average velocity to the axial velocity, m/s

v Velocity, m/s

\bar{v}	Average velocity, m/s
W	Channel width, μm
x	Position coordinate, m
\vec{x}	Position vector of the particles, m
y	Position coordinate, m
y_i	Molar fraction
z	Position coordinate, m

Greek symbols

ξ	Time period, s
μ	Viscosity, Pa·s
ρ	Density, kg/m^3

References

- [1] D. Reay, C. Ramshaw, A. Harvey, *Process Intensification*, 2013.
<https://doi.org/10.1016/B978-0-08-098304-2.00005-5>.
- [2] A.I. Stankiewicz, J.A. Moulijn, *Process intensification: Transforming chemical engineering*, *Chem. Eng. Prog.* 96 (2000) 22–33.
<https://doi.org/10.1002/btpr.305>.
- [3] J.A. Moulijn, A. Stankiewicz, J. Grievink, A. Górak, *Process intensification and process systems engineering: A friendly symbiosis*, *Comput. Chem. Eng.* 32 (2008) 3–11. <https://doi.org/10.1016/j.compchemeng.2007.05.014>.
- [4] P. Rojahn, V. Hessel, K.D.P. Nigam, F. Schael, *Applicability of the axial dispersion model to coiled flow inverters containing single liquid phase and segmented liquid-liquid flows*, *Chem. Eng. Sci.* 182 (2018) 77–92.
<https://doi.org/10.1016/j.ces.2018.02.031>.
- [5] Norbert Kockmann, *Micro Process Engineering*, Wiley-VCH Verlag GmbH,

- Weinheim, Germany, 2006. <https://doi.org/10.1002/9783527616749>.
- [6] P.L. Mills, D.J. Quiram, J.F. Ryley, Microreactor technology and process miniaturization for catalytic reactions — A perspective on recent developments and emerging technologies, *62* (2007) 6992–7010.
<https://doi.org/10.1016/j.ces.2007.09.021>.
- [7] V. Kumar, K.D.P. Nigam, Process intensification in green synthesis, *Green Process. Synth.* 1 (2012) 79–107. <https://doi.org/10.1515/greenps-2011-0003>.
- [8] A.D. Stroock, Chaotic Mixer for Microchannels, *Scienc.* 295 (2002) 647–651.
<https://doi.org/10.1126/science.1066238>.
- [9] M.A. Ansari, K.Y. Kim, Shape optimization of a micromixer with staggered herringbone groove, *Chem. Eng. Sci.* 62 (2007) 6687–6695.
<https://doi.org/10.1016/j.ces.2007.07.059>.
- [10] J. Aubin, D.F. Fletcher, C. Xuereb, Design of micromixers using CFD modelling, in: *Chem. Eng. Sci.*, 2005: pp. 2503–2516.
<https://doi.org/10.1016/j.ces.2004.11.043>.
- [11] A. Cantu-Perez, M. Al-Rawashdeh, V. Hessel, A. Gavriilidis, Reaction modelling of a microstructured falling film reactor incorporating staggered herringbone structures using eddy diffusivity concepts, *Chem. Eng. J.* 227 (2013) 34–41.
<https://doi.org/10.1016/j.cej.2012.11.122>.
- [12] D.G. Hassell, W.B. Zimmerman, Investigation of the convective motion through a staggered herringbone micromixer at low Reynolds number flow, *Chem. Eng. Sci.* 61 (2006) 2977–2985. <https://doi.org/10.1016/j.ces.2005.10.068>.

- [13] S.P. Kee, A. Gavriilidis, Design and characterisation of the staggered herringbone mixer, *Chem. Eng. J.* 142 (2008) 109–121.
<https://doi.org/10.1016/j.cej.2008.02.001>.
- [14] Y.Z. Liu, B.J. Kim, H.J. Sung, Two-fluid mixing in a microchannel, *Int. J. Heat Fluid Flow.* 25 (2004) 986–995.
<https://doi.org/10.1016/j.ijheatfluidflow.2004.03.006>.
- [15] A.D. Stroock, G.J. McGraw, Investigation of the staggered herringbone mixer with a simple analytical model, *Philos. Trans. R. Soc. London A Math. Phys. Eng. Sci.* 362 (2004) 971–986. <https://doi.org/10.1098/rsta.2003.1357>.
- [16] M. Wiese, S. Benders, B. Blümich, M. Wessling, 3D MRI velocimetry of non-transparent 3D-printed staggered herringbone mixers, *Chem. Eng. J.* 343 (2018) 54–60. <https://doi.org/10.1016/j.cej.2018.02.096>.
- [17] Z. Sun, W. Li, X. Ma, Z. Ayub, Y. He, Flow boiling in horizontal annuli outside horizontal smooth, herringbone and three-dimensional enhanced tubes, *Int. J. Heat Mass Transf.* (2019).
<https://doi.org/10.1016/j.ijheatmasstransfer.2019.118554>.
- [18] J. Marschewski, R. Brechbühler, S. Jung, P. Ruch, B. Michel, D. Poulikakos, Significant heat transfer enhancement in microchannels with herringbone-inspired microstructures, *Int. J. Heat Mass Transf.* 95 (2016) 755–764.
<https://doi.org/10.1016/j.ijheatmasstransfer.2015.12.039>.
- [19] A. Afzal, K.-Y. Kim, Three-objective optimization of a staggered herringbone micromixer, *Sensors Actuators B Chem.* 192 (2014) 350–360.
<https://doi.org/10.1016/j.snb.2013.10.109>.

- [20] M. Al-Rawashdeh, A. Cantu-Perez, D. Ziegenbalg, P. Löb, A. Gavriilidis, V. Hessel, F. Schönfeld, Microstructure-based intensification of a falling film microreactor through optimal film setting with realistic profiles and in-channel induced mixing, *Chem. Eng. J.* 179 (2012) 318–329.
<https://doi.org/10.1016/j.cej.2011.11.014>.
- [21] J. Marschewski, S. Jung, P. Ruch, N. Prasad, S. Mazzotti, B. Michel, D. Poulikakos, Mixing with herringbone-inspired microstructures: overcoming the diffusion limit in co-laminar microfluidic devices, *Lab Chip*. 15 (2015) 1923–1933. <https://doi.org/10.1039/C5LC00045A>.
- [22] J.T. Adeosun, A. Lawal, Residence-time distribution as a measure of mixing in T-junction and multilaminated/elongational flow micromixers, *Chem. Eng. Sci.* 65 (2010) 1865–1874. <https://doi.org/10.1016/j.ces.2009.11.038>.
- [23] A. Cantu-Perez, S. Bi, S. Barrass, M. Wood, A. Gavriilidis, Residence time distribution studies in microstructured plate reactors, *Appl. Therm. Eng.* 31 (2011) 634–639. <https://doi.org/10.1016/J.APPLTHERMALENG.2010.04.024>.
- [24] A.K. Saxena, K.D.P. Nigam, Laminar dispersion in helically coiled tubes of square cross-section, *Can. J. Chem. Eng.* 61 (1983) 53–57.
<https://doi.org/10.1002/cjce.5450610109>.
- [25] A. Cantu-Perez, S. Barrass, A. Gavriilidis, Residence time distributions in microchannels: Comparison between channels with herringbone structures and a rectangular channel, *Chem. Eng. J.* 160 (2010) 834–844.
<https://doi.org/10.1016/j.cej.2009.07.023>.
- [26] J.D. Kirtland, G.J. McGraw, A.D. Stroock, Mass transfer to reactive boundaries

- from steady three-dimensional flows in microchannels, *Phys. Fluids*. 18 (2006) 073602. <https://doi.org/10.1063/1.2222389>.
- [27] S.K. Yoon, G.W. Fichtl, P.J.A. Kenis, Active control of the depletion boundary layers in microfluidic electrochemical reactors, *Lab Chip*. 6 (2006) 1516. <https://doi.org/10.1039/b609289f>.
- [28] J.P. Golden, T.M. Floyd-Smith, D.R. Mott, F.S. Ligler, Target delivery in a microfluidic immunosensor, *Biosens. Bioelectron.* 22 (2007) 2763–2767. <https://doi.org/10.1016/j.bios.2006.12.017>.
- [29] M. Lopez, M.D. Graham, Enhancement of mixing and adsorption in microfluidic devices by shear-induced diffusion and topography-induced secondary flow, *Phys. Fluids*. 20 (2008). <https://doi.org/10.1063/1.2912136>.
- [30] V. Kumar, M. Paraschivoiu, K.D.P. Nigam, Single-phase fluid flow and mixing in microchannels, *Chem. Eng. Sci.* 66 (2011) 1329–1373. <https://doi.org/10.1016/j.ces.2010.08.016>.
- [31] V. Kumar, V. Shirke, K.D.P. Nigam, Performance of Kenics static mixer over a wide range of Reynolds number, *Chem. Eng. J.* 139 (2008) 284–295. <https://doi.org/10.1016/j.cej.2007.07.101>.
- [32] R.K. Thakur, C. Vial, K.D.P. Nigam, E.B. Nauman, G. Djelveh, Static Mixers in the Process Industries—A Review, *Chem. Eng. Res. Des.* 81 (2003) 787–826. <https://doi.org/10.1205/026387603322302968>.
- [33] K.D.P. Nigam, E.B. Nauman, Residence time distributions of power law fluids in motionless mixers, *Can. J. Chem. Eng.* (1985).

<https://doi.org/10.1002/cjce.5450630322>.

- [34] P. Joshi, K.D.P. Nigam, E.B. Nauman, The Kenics static mixer: new data and proposed correlations, *Chem. Eng. J. Biochem. Eng. J.* (1995).
[https://doi.org/10.1016/0923-0467\(94\)02948-2](https://doi.org/10.1016/0923-0467(94)02948-2).
- [35] H.E.H. Meijer, M.K. Singh, P.D. Anderson, On the performance of static mixers: A quantitative comparison, *Prog. Polym. Sci.* 37 (2012) 1333–1349.
<https://doi.org/10.1016/j.progpolymsci.2011.12.004>.
- [36] F. Ruiz-Ruiz, E. López-Guajardo, P. Vázquez-Villegas, M.E. del Angel-Chong, K.D.P. Nigam, R.C. Willson, M. Rito-Palomares, Continuous aqueous two-phase extraction of microalgal C-phycoyanin using a coiled flow inverter, *Chem. Eng. Process. - Process Intensif.* 142 (2019) 107554.
<https://doi.org/10.1016/j.cep.2019.107554>.
- [37] M. Mridha, K.D.P. Nigam, Coiled flow inverter as an inline mixer, *Chem. Eng. Sci.* 63 (2008) 1724–1732. <https://doi.org/10.1016/j.ces.2007.10.028>.
- [38] A.K. Saxena, K.D.P. Nigam, Coiled configuration for flow inversion and its effect on residence time distribution, *AIChE J.* 30 (1984) 363–368.
<https://doi.org/10.1002/aic.690300303>.
- [39] D. Rossi, L. Gargiulo, G. Valitov, A. Gavriilidis, L. Mazzei, Experimental characterization of axial dispersion in coiled flow inverters, *Chem. Eng. Res. Des.* 120 (2017) 159–170. <https://doi.org/10.1016/j.cherd.2017.02.011>.
- [40] F. Schönfeld, S. Hardt, Simulation of Helical Flows in Microchannels, *AIChE J.* 50 (2004) 771–778. <https://doi.org/10.1002/aic.10071>.

- [41] S. Soni, L. Sharma, P. Meena, S. Roy, K.D.P. Nigam, Compact coiled flow inverter for process intensification, *Chem. Eng. Sci.* 193 (2019) 312–324.
<https://doi.org/10.1016/j.ces.2018.09.008>.
- [42] E. López-Guajardo, E. Ortiz-Nadal, A. Montesinos-Castellanos, K.D.P. Nigam, Coiled flow inverter as a novel alternative for the intensification of a liquid-liquid reaction, *Chem. Eng. Sci.* 169 (2017) 179–185.
<https://doi.org/10.1016/j.ces.2017.01.016>.
- [43] J. Singh, V. Srivastava, K.D.P. Nigam, Novel Membrane Module for Permeate Flux Augmentation and Process Intensification, *Ind. Eng. Chem. Res.* 55 (2016) 3861–3870. <https://doi.org/10.1021/acs.iecr.5b04865>.
- [44] M.M. Mandal, P. Aggarwal, K.D.P. Nigam, Liquid–Liquid Mixing in Coiled Flow Inverter, *Ind. Eng. Chem. Res.* 50 (2011) 13230–13235.
<https://doi.org/10.1021/ie2002473>.
- [45] C.P. Tiwari, F. Delgado-Licona, M. Valencia-Llompart, S. Nuñez-Correa, K.D.P. Nigam, A. Montesinos-Castellanos, E.A. López-Guajardo, A. Aguirre-Soto, Shining Light on the Coiled-Flow Inverter—Continuous-Flow Photochemistry in a Static Mixer, *Ind. Eng. Chem. Res.* 59 (2020) 3865–3872.
<https://doi.org/10.1021/acs.iecr.9b05008>.
- [46] R. Baber, L. Mazzei, N.T.K. Thanh, A. Gavriilidis, An engineering approach to synthesis of gold and silver nanoparticles by controlling hydrodynamics and mixing based on a coaxial flow reactor, *Nanoscale.* 9 (2017) 14149–14161.
<https://doi.org/10.1039/C7NR04962E>.
- [47] E.B. Nauman, Enhancement of heat transfer and thermal homogeneity with

- motionless mixers, *AIChE J.* 25 (1979) 246–258.
<https://doi.org/10.1002/aic.690250206>.
- [48] V. Kumar, M. Mridha, A.K. Gupta, K.D.P. Nigam, Coiled flow inverter as a heat exchanger, *Chem. Eng. Sci.* 62 (2007) 2386–2396.
<https://doi.org/10.1016/J.CES.2007.01.032>.
- [49] V. Kumar, Vikash, K.D.P. Nigam, Multiphase fluid flow and heat transfer characteristics in microchannels, *Chem. Eng. Sci.* (2017).
<https://doi.org/10.1016/j.ces.2017.01.018>.
- [50] H. Wang, P. Iovenitti, E. Harvey, S. Masood, Numerical investigation of mixing in microchannels with patterned grooves, *J. Micromechanics Microengineering.* 13 (2003) 801–808. <https://doi.org/10.1088/0960-1317/13/6/302>.
- [51] J. Aubin, D.F. Fletcher, J. Bertrand, C. Xuereb, Characterization of the mixing quality in micromixers, *Chem. Eng. Technol.* 26 (2003) 1262–1270.
<https://doi.org/10.1002/ceat.200301848>.
- [52] C.W. Gardiner, *Handbook of stochastic methods for physics, chemistry, and the natural sciences*, Springer-Verlag, 1985.
- [53] T.K. Sherwood, R.L. Pigford, C.R. Wilke, *Mass transfer*, McGraw-Hill, 1975.
- [54] J.M. MacInnes, A. Vikhansky, R.W.K. Allen, Numerical characterisation of folding flow microchannel mixers, *Chem. Eng. Sci.* (2007).
<https://doi.org/10.1016/j.ces.2007.02.014>.
- [55] J.S. Son, T.J. Hanratty, Limiting relation for the eddy diffusivity close to a wall, *AIChE J.* 13 (1967) 689–696. <https://doi.org/10.1002/aic.690130419>.

- [56] D.A. Shaw, T.J. Hanratty, Turbulent mass transfer rates to a wall for large Schmidt numbers, *AIChE J.* 23 (1977) 28–37.
<https://doi.org/10.1002/aic.690230106>.
- [57] B.M. Mitrovic, P.M. Le, D. V. Papavassiliou, On the Prandtl or Schmidt number dependence of the turbulent heat or mass transfer coefficient, *Chem. Eng. Sci.* 59 (2004) 543–555. <https://doi.org/10.1016/j.ces.2003.09.039>.
- [58] A. Cantu-Perez, S. Kee, A. Gavriilidis, Mixing and Residence Time Distribution Studies in Microchannels with Floor Herringbone Structures, *Proceedings of the COMSOL Conference, Hannover* (2008).

Figures

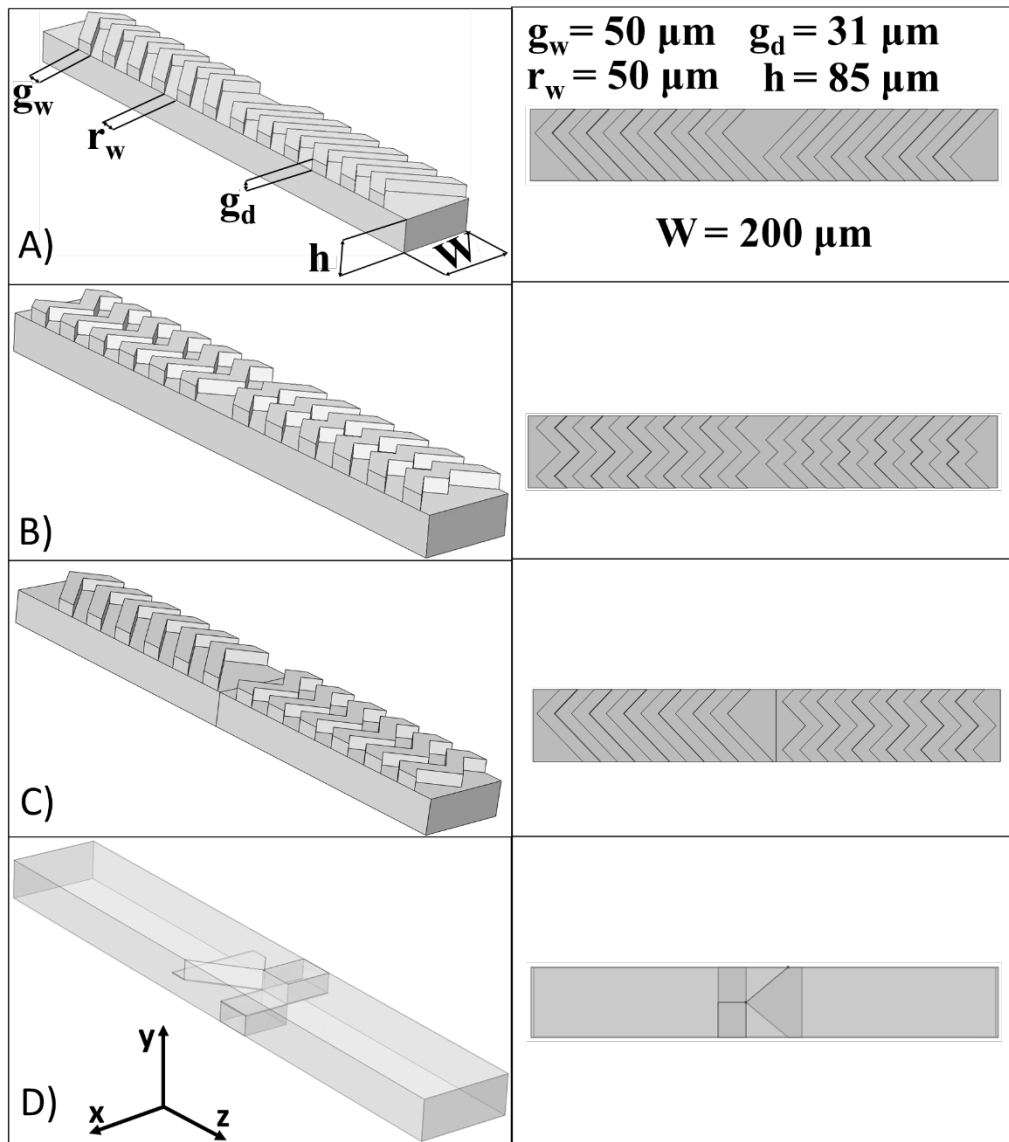


Figure 1.

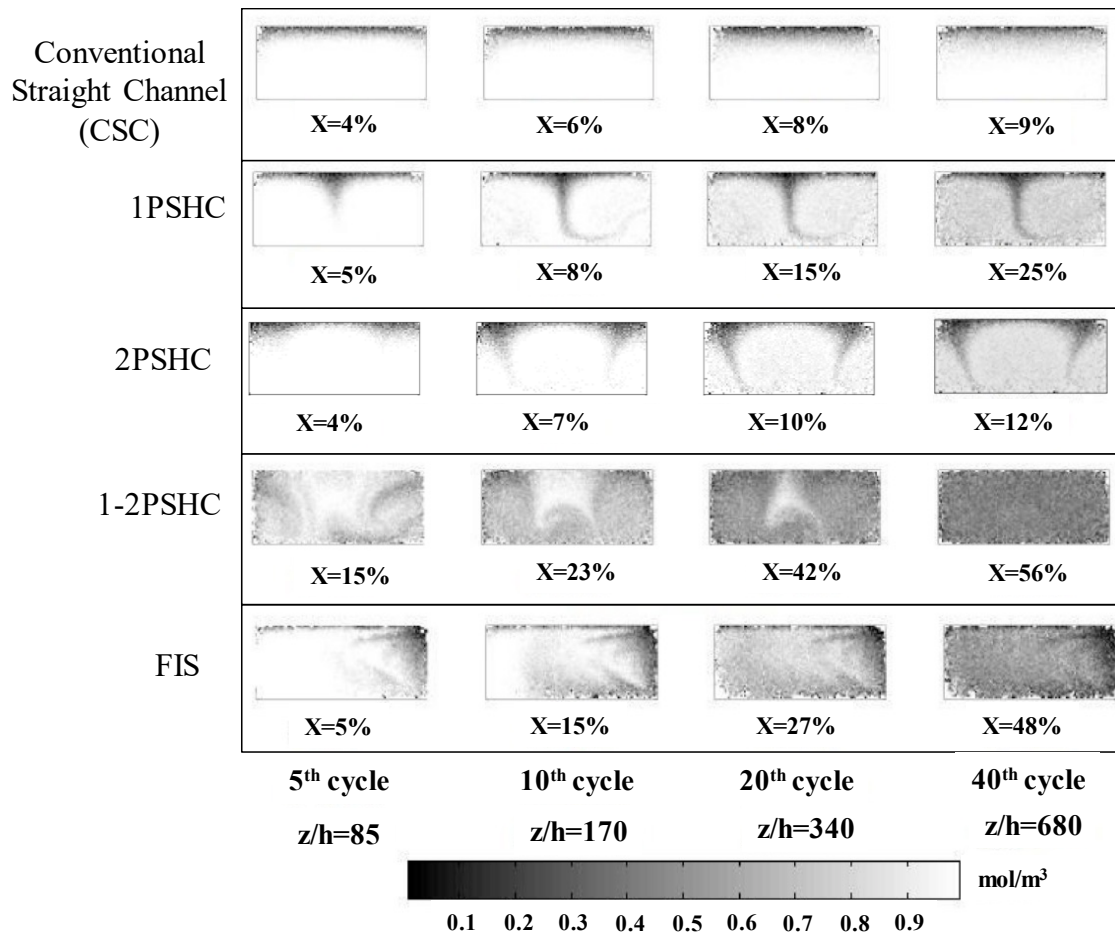


Figure 2.

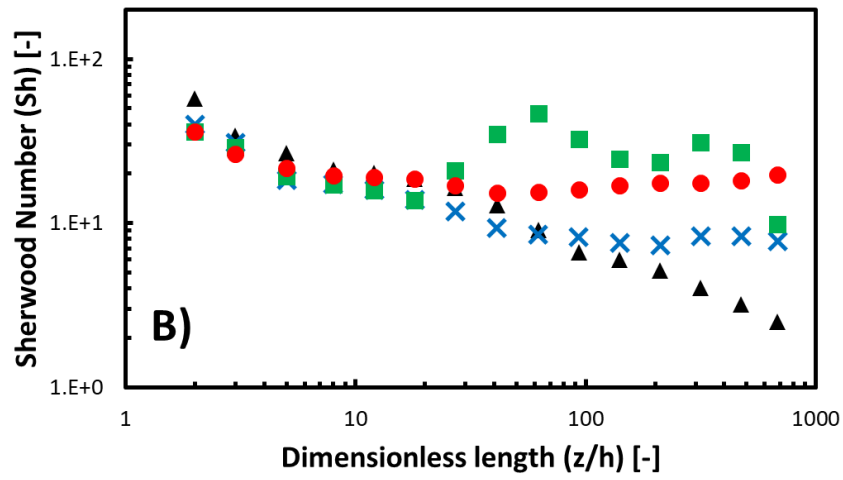
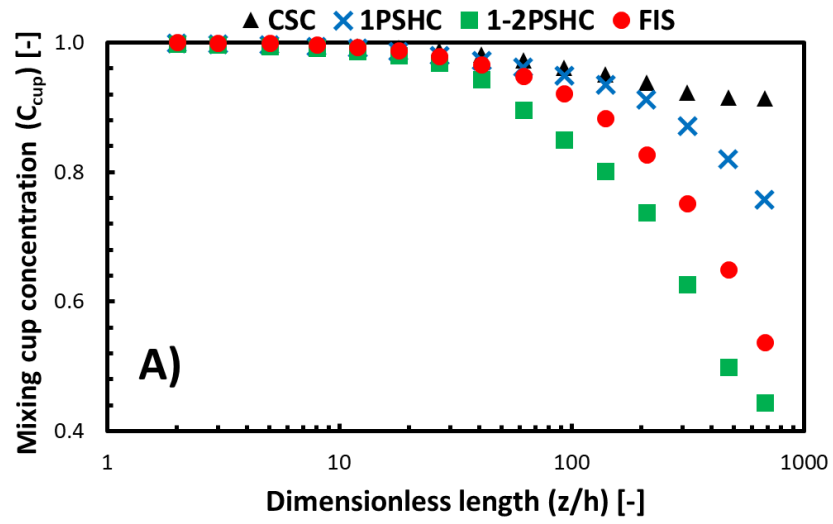


Figure 3.

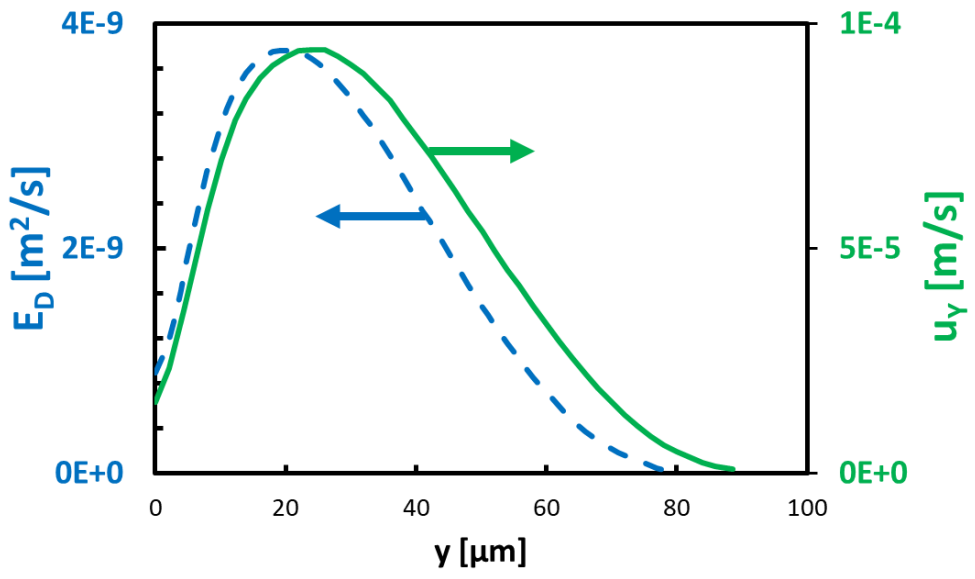


Figure 4.

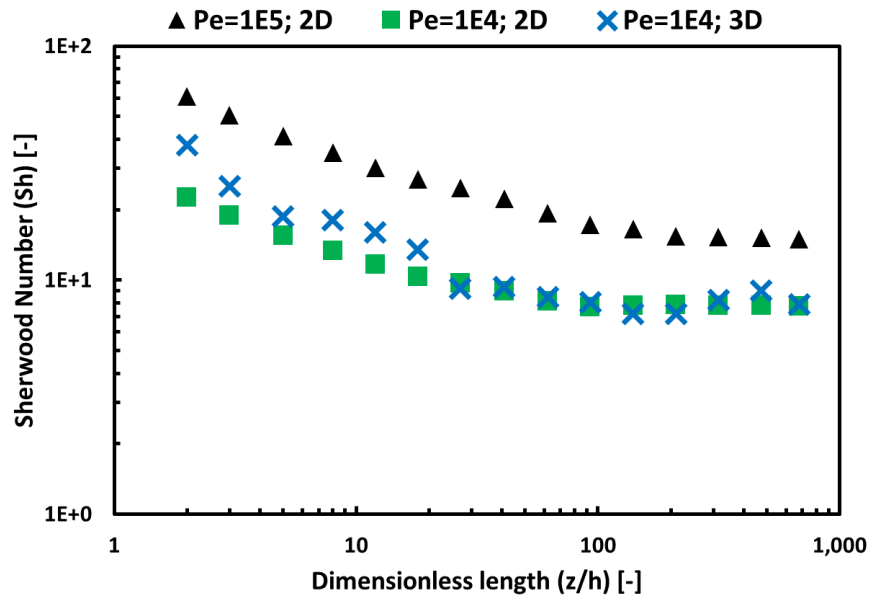


Figure 5.

Figures List

- Figure 1 Geometries considered for the numerical analysis of mass transfer to a reacting wall: A) Staggered 1-peak herringbone channel; B) Staggered 2-peak herringbone channel; C) Flow inversion geometry for reaction studies. The flow direction is as the positive z-axis
- Figure 2 Cross-sectional reactant concentration maps and reactant conversion X , at different lengths for CRC, 1PSHC, 2PSHC, 1-2PSHC and FIS. $Pe = 10^4$
- Figure 3 A) Mixing cup concentration at different lengths for various microchannel geometries. B) Sherwood number at different lengths. $Pe = 10^4$. Note that 1 cycle is approximately $z/h = 17$.
- Figure 4 Vertical velocity (\bar{u}_y) and virtual eddy diffusivity (ED) as a function of channel vertical coordinate for the 1PSHC. The reactive wall is located at a channel height of $85 \mu\text{m}$. $Pe = 10^4$.
- Figure 5 Sherwood number vs. dimensionless length comparison for 3D particle tracking approach with 2D virtual eddy diffusivity approach.